Published in final edited form as:
Cell. 2011 January 7; 144(1): 119–131. doi:10.1016/j.cell.2010.12.014.

Tunable signal processing in synthetic MAP kinase cascades

Ellen C. O'Shaughnessy[1], **Santhosh Palani**[2], **James J. Collins**[1,4,*], and **Casim A. Sarkar**[2,3,*]

[1]Howard Hughes Medical Institute and Department of Biomedical Engineering, Center for BioDynamics and Center for Advanced Biotechnology, Boston University, 44 Cummington Street, Boston, MA 02215, USA

[2]Department of Bioengineering, University of Pennsylvania, 210 S. 33rd Street, Philadelphia, PA 19104, USA

[3]Department of Chemical and Biomolecular Engineering, University of Pennsylvania, 220 S. 33rd Street, Philadelphia, PA 19104, USA

[4]Wyss Institute for Biologically Inspired Engineering, Harvard University, Boston, MA 02115, USA

SUMMARY

The flexibility of MAPK cascade responses enables regulation of a vast array of cell-fate decisions, but elucidating the mechanisms underlying this plasticity is difficult in endogenous signaling networks. We constructed insulated mammalian MAPK cascades in yeast to explore how intrinsic and extrinsic perturbations affect the flexibility of these synthetic signaling modules. Contrary to biphasic dependence on scaffold concentration, we observe monotonic decreases in signal strength as scaffold concentration increases. We find augmenting the concentration of sequential kinases can enhance ultrasensitivity and lower the activation threshold. Further, integrating negative regulation and concentration variation can decouple ultrasensitivity and threshold from the strength of the response. Computational analyses show that cascading can generate ultrasensitivity and that natural cascades with different kinase concentrations are innately biased toward their distinct activation profiles. This work demonstrates that tunable signal processing is inherent to minimal MAPK modules and elucidates principles for rational design of synthetic signaling systems.

INTRODUCTION

MAPK pathways are ubiquitous, versatile signaling modules found in all eukaryotic cells. They transmit and process signals regulating a broad array of cell-fate decisions, including proliferation, differentiation, motility, stress-responses and apoptosis (Avruch, 2007). While several MAPK families have been elucidated, all consist of three sequential kinases activated by dual, non-processive phosphorylation events. The biological design principles underlying a three-tiered cascade structure have been the subject of vigorous debate for many years. A number of hypotheses have been put forth to account for the use of multi-step signaling pathways including signal amplification, increased signaling speed, multiple points of regulation, noise tolerance and the generation of switch-like responses (Chen and Thorner, 2005). While it is likely that this heavily conserved pathway has evolved to serve

*Co-corresponding authors: casarkar@seas.upenn.edu, jcollins@bu.edu.

multiple purposes, its structure clearly enables great flexibility of system response. Extensive experimental work on MAPK cascades has shown that responses can be graded or switch-like (ultrasensitive), transient or sustained, and monostable or bistable (Bhalla et al., 2002; Huang and Ferrell, 1996; Poritz et al., 2001; Santos et al., 2007).

A growing body of research has demonstrated that the systems-level properties of MAPK activation vary greatly depending on cellular context and that the characteristics of this activation can determine cell fate. Seminal work on the activation of p42 MAPK in *X. laevis* demonstrated steep ultrasensitivity (Ferrell and Machleder, 1998; Huang and Ferrell, 1996), while studies of MAPK cascades in *S. cerevisiae* revealed graded activation profiles (Poritz et al., 2001). A series of studies in mammalian systems showed that different cell types exhibit either switch-like (Bagowski et al., 2003; Harding et al., 2005) or proportional (Mackeigan et al., 2005; Whitehurst et al., 2004) activation responses. Even within the same cell type, an individual MAPK cascade can exhibit different dynamic responses that lead to distinct cell fates. In PC12 cells, MAPK activation is transient and graded when stimulated with epidermal growth factor, leading to proliferation. In contrast, nerve growth factor stimulation results in cell differentiation through sustained and ultrasensitive MAPK activation (Marshall, 1995; Santos et al., 2007). Recent work has shown that altering the activation profile of MAPK in these cells is sufficient to reverse the stimulus-phenotype relationship (Santos et al., 2007). Further, in BHK cells, tethering the MAPK module to the plasma membrane can lower the threshold of activation and consequently the percentage of cells that differentiate depends upon both the stimulus magnitude and the location of the cascade in the cell (Harding et al., 2005). Finally, it has been shown that activation of MAPK in NIH-3T3 fibroblasts is dependent upon temporal dynamics of the stimulus (Bhalla et al., 2002). Naïve cells exhibit bistable MAPK activation in response to platelet-derived growth factor while previously stimulated cells show proportional, monotonic activation. It has been proposed that this desensitization enables the downregulation of MAPK activity, a molecule whose prolonged stimulation can be deleterious.

It is clear from both experimental and theoretical work that the behavior of MAPK cascades *in vivo* is dictated in part by multiple levels of feedback regulation. In particular, bistability, an essential characteristic in many cell-fate decisions, arises through feedback. However, feedback alone is not sufficient to achieve bistability. Bistable responses require a nonlinearity in the system, feedback to reinforce the nonlinearity and proper balance between the system components (Ferrell and Xiong, 2001). Ultrasensitivity in MAPK activation is a critical, systems-level property as it can serve as the fundamental nonlinearity required to achieve stable, potentially irreversible, cellular decisions. Indeed, several experimental studies of bistable MAPK activation report ultrasensitive activation profiles as well (Bhalla et al., 2002; Ferrell and Machleder, 1998; Santos et al., 2007). Dissecting the contributions of ultrasensitivity and feedback to a specific bistable response is often untenable in the context of complex endogenous signaling networks.

Many biological systems are organized into functional modules that perform key steps in a larger process (Hartwell et al., 1999). It is often difficult to characterize the potential behaviors of these component subsystems *in vivo* because of interconnectivity and complex layers of regulation found in biological systems. This is particularly true in signaling networks, which exhibit multifaceted regulation such as feedback, localization and extensive, functional cross-talk (Natarajan et al., 2006). Nonetheless, interpreting, influencing and predicting how complex networks carry out biological functions depends critically upon our understanding of their component modules. Here we use a synthetic biology approach to obviate the challenges of interconnectivity in uncovering the inherent capabilities of the MAPK module; we do so by systematically applying intrinsic and extrinsic perturbations to tune the activation dynamics of a minimal, well-insulated cascade.

By studying an isolated module, we develop a mechanistic understanding of the effects of these perturbations both experimentally and computationally.

In the present study, we built an exogenous, minimal MAPK cascade to investigate the effects of extrinsic and intrinsic regulators on the plasticity of this isolated signaling module. We expressed the mammalian Raf-MEK-ERK cascade in the yeast *S. cerevisiae*, and applied the intrinsic perturbation of concentration variation between cascade members and the extrinsic perturbations of scaffolding and negative regulation. We show that varying the relative concentrations of MEK and ERK confers great flexibility of the system response and may prime the cascade for either low or high ultrasensitivity. Strikingly, the *X. laevis* p42 MAPK cascade that shows sharp ultrasensitivity and the *S. cerevisiae* pheromone pathway that is more graded both fit well within the theoretical framework generated by this novel intrinsic perturbation. Additionally, we identify cascading itself as a novel, concentration-dependent mechanism, for generating ultrasensitivity. We further demonstrate that, in contrast to a biphasic dependence on scaffold concentration (prozone effect), expression of a two-member scaffold results in a monotonic dependence of signal strength on scaffold concentration, with a sharp reduction observed at high concentration. Finally, introducing negative regulation of either MEK or ERK leads to a reduction in ultrasensitivity and an increase in threshold, even in the absence of feedback. We used a computational model to integrate these intrinsic and extrinsic perturbations over a large parameter space and found regions in which signal characteristics can be tuned independently. Experimentally, we demonstrate the decoupling of signal strength from the ultrasensitivity and threshold of the response. Thus, through the use of a synthetic signaling module, we identified novel mechanisms for generating ultrasensitivity, elucidated cellular strategies for tuning the activation of the system and highlighted regulatory principles that can be used in designing artificial signaling networks.

RESULTS

The Basic Synthetic Cascade

We constructed a basic synthetic cascade using the mammalian pathway of Raf-MEK-ERK (Figure 1A) in which the Raf level of the cascade is a hormone binding domain fusion protein, eGFP:ΔRaf-1:ER-DD (Raf:ER), whose kinase activity is modulated by the addition of β-estradiol (McMahon, 2001). Consequently, the entire cascade is cytosolic (Figure S1) and does not depend upon receptor-mediated membrane recruitment for activation. Single integrated copies of wild-type, epitope-tagged Raf:ER, c-myc-MEK1 (MEK) and His_6-ERK2 (ERK) were co-expressed from different auxotrophic loci by a reverse tTA-driven expression system (P_{tetO7}) (Bellí et al., 1998) induced with anhydrotetracycline (aTC). The system was stimulated with estradiol and assayed for steady-state activated ERK directly with quantitative western blotting (Figure 1B) to eliminate additional signal processing steps such as transcriptional activation (Mackeigan et al., 2005). As designed, our system is not bistable as it does not fulfill the requirements of non-linearity, feedback and proper balance and therefore the population mean reflects the unique activation state of the system. When the three kinases were expressed at equal concentration levels, the system reached a half-maximal response (EC50) at 32 ± 1.4 nM and exhibited moderate ultrasensitivity (Figure 1C). The apparent Hill coefficient attained by this basic, constant-expression cascade, n_H=1.8 ± 0.13, fits well within the range of sensitivities observed in natural systems.

An ordinary differential equation (ODE) model of the basic cascade based on mass-action kinetics (Huang and Ferrell, 1996) accurately captures the response (Figure 1C). All parameters and initial conditions were refined from literature values by globally fitting the Hill coefficient, signal strength and EC50 to the experimental steady-state response curves of the basic and variable expression cascades (Supplemental Text). Parameter values were

then held constant in simulating subsequent perturbations. The model assumes non-processive, dual-step phosphorylation events between sequential kinases, as has been demonstrated experimentally (Burack and Sturgill, 1997).

Insulation of this exogenous cascade from the host was assayed by a variety of methods. We identified possible interaction pathways by homology (Avruch, 2007) and previous findings in the literature (Atienza, 2000), and consequently designed pathway-specific transcriptional reporters for the pheromone, invasive growth and cell wall integrity pathways in *S. cerevisiae*. The synthetic cascade was stimulated with estradiol, and expression of tdTomato from each native pathway-specific promoter was determined by flow cytometry. We found minimal transcriptional activation from each of the endogenous pathways assayed when compared with pathway-specific positive controls (Figure 1D). In addition, we stimulated cells with agonists of endogenous MAPK pathways, including α-factor (Bashor et al., 2008), glucose depletion (Cullen and Sprague, 2000) and caffeine (Jung et al., 2002), and determined the activation level of the synthetic MAPK cascade. We found almost no phosphorylation of ERK in response to glucose starvation and caffeine, and ~15% activation in response to α-factor, despite the significant impact these stimuli have on diverse cellular processes (Figure 1E). Further, we assayed for dephosphorylation of the synthetic cascade by endogenous phosphatases and found very modest interaction with these negative regulators (Figure S1). Taken together, these data indicate that the synthetic cascade is well insulated from the host and the dynamic responses we observe are a result of the minimal system itself and do not arise from unknown endogenous effectors.

The Variable Expression Cascades

In natural systems, Raf, MEK and ERK are present at different concentrations, frequently increasing for sequential kinases. Further, the relative concentrations of cascade members vary significantly across different experimental systems (Ferrell, 1996). To understand the systems-level effects of this intrinsic perturbation, we constructed a cascade increasing the kinase concentration of each subsequent step, achieving ~10- fold difference across the entire cascade (Figure 2A). Concentration was varied by expressing a single, integrated copy of Raf:ER with P_{tetO7}, high-copy MEK with P_{tetO7}, and high-copy ERK from the Gal1 promoter (P_{Gal}) induced with galactose. The concentration range of this synthetic system was initially determined computationally by a global fit to the basic and variable cascades and was verified experimentally by quantitative ELISA against ERK (Figure S2). Under this perturbation we found that the ultrasensitivity increased from $n_H = 1.8 \pm 0.13$ to 2.8 ± 0.19, while the threshold was reduced from 32 ± 1.4 nM to 6.6 ± 0.14 nM (Figure 2B).

Qualitatively, this response is captured well by our computational model (Figure 2C). Interestingly, for this experimentally attainable range of parameter values, the model predicts that the MEK concentration will have a greater effect than that of ERK on both the ultrasensitivity and threshold of the response. We computationally varied MEK and ERK from 10nM to 100nM and determined the Hill coefficient and EC50 of each activation response (Figure 2D,E). The slope of the resulting surfaces is steeper when MEK is varied for a fixed value of ERK than when ERK is varied for a fixed MEK value. Therefore, we hypothesized that reducing the concentration of MEK in our variable cascade would increase the threshold and reduce the ultrasensitivity of the response.

To test this hypothesis, we built a variable expression cascade with a concentration of MEK in between those in the basic and original variable cascades (Figure 2F). In this low-MEK variable cascade, MEK was expressed from a single-integrated copy by P_{Gal} while the Raf:ER and ERK levels were kept the same in the two variable cascades. As predicted, lowering MEK expression resulted in both a reduction in ultrasensitivity from $n_H = 2.8 \pm$

0.19 to 2.0 ± 0.19 and an increase in threshold from EC50 = 6.6 ± 0.14 nM to 15 ± 0.78 nM when compared with the high-MEK cascade (Figure 2B and 2F).

The Basic Cascade with Scaffolding

Scaffolding has been shown to be critical to signal transduction for some MAPK pathways (Elion, 2001), while in others the effects of co-localization remain unclear (Kolch, 2005). Furthermore, it is evident that scaffold concentration can be a strong determinant of MAPK activation (Burack and Shaw, 2000; Levchenko et al., 2000; Locasale et al., 2007). Therefore, we co-expressed the basic cascade with a modified two-member (MEK and ERK) scaffold, paxillin^{Y118D} (pax*), and varied the scaffold concentration from ~ 30nM to 100nM by expression from single-copy and high-copy P_{Gal} (Figure 3A). Association of ERK and wild-type paxillin is regulated by phosphorylation of Tyr^{118} (Ishibe et al., 2003), which we mimicked with mutation to Asp and verified by co-immunoprecipitation (Figure S3). We found that moderate expression of pax* from single-copy P_{Gal} results in a slight reduction in ultrasensitivity and a marginal effect on signal strength (Figure 3B). In contrast, we observed a marked decrease in signal strength, to approximately 25% unscaffolded levels, when pax* is co-expressed from high-copy P_{Gal}. These results demonstrate that the Raf-MEK-ERK cascade is inherently catalytically efficient and does not depend on scaffolding to effectively propagate a signal. This is in contrast to some native yeast MAPK cascades, such as the mating and high osmolarity pathways, that require scaffolding (Qi, 2005). Furthermore, our findings show that, when expressed near stoichiometric ratios optimal for signal propagation (Levchenko et al., 2000), scaffolding has a negligible effect on signal strength compared to that of the basic cascade.

In addition to a reduction in signal strength, we observed a two-phase dose-response in the presence of high scaffold concentrations (Figure 3C). Though paxillin is not homologous to native yeast MAPK scaffolds, exogenous paxillin has previously been shown to localize strongly to sites of polarized growth in yeast (Gao et al., 2004). Therefore, we hypothesized that this complex behavior arises from sequestration of the MAPK cascade, and we tested this hypothesis by explicitly including compartmentalization in our model of the basic cascade to generate a scaffold model. We found a single-phase ERK activation profile at moderate scaffold levels and a biphasic dose-response at high scaffold concentrations (Figure 3C,D). This multi-phase response could not be generated with either a well-mixed model or a compartmental model in which paxillin cannot bind ERK (Figure S3), suggesting that sequestration of the cascade is necessary to elicit the observed response.

The Basic Cascade with Negative Regulation

In natural MAPK cascades, sequential activation by kinases is balanced by inactivation through negative regulation. Both theoretical (Heinrich et al., 2002) and experimental (Hornberg et al., 2005) work has demonstrated that activation and deactivation processes control distinct aspects of the MAPK response. Further, it has been shown that high concentrations of phosphatase can convert an ultrasensitive, bistable MAPK response into a proportional, transient activation profile via the disruption of positive feedback (Bhalla et al., 2002). We hypothesized that, even in the absence of feedback, the presence of negative regulators would tune the activation profile of the MAPK response. We independently introduced two modes of negative regulation to a purely kinase-based cascade to test this hypothesis. First, we co-expressed the basic cascade with a weak, cytosolically-targeted ERK phosphatase, MKP-$1^{L16A/L17A}$ (MKP1-cyt) (Wu et al., 2005), from single-copy P_{Gal} (Figure 4A). The presence of this dual-specificity phosphatase affected not only the threshold of the system which increased from 32 ± 1.4 nM to 110 ± 9.3 nM, but also the ultrasensitivity which was reduced from n_H = 1.8 ± 0.13 to 1.2 ± 0.11 (Figure 4B). A model

of the basic cascade with this additional enzymatic reaction predicted both of these features qualitatively (Figure 4C).

In addition to enzymatic negative regulation of ERK, we perturbed the system with the small-molecule MEK inhibitor, CI-1040 (Figure 4D). CI-1040 is a strong non-competitive, but reversible, binder that targets the unphosphorylated form of MEK and renders the kinase catalytically inactive (Ohren et al., 2004). We found similar results to co-expression of MKP1-cyt in that the Hill coefficient decreased from 1.8 ± 0.13 to 1.1 ± 0.12 in the presence of 50nM CI-1040 and the threshold increased from 32 ± 1.4 nM to 120 ± 10 nM (Figure 4E). A model of the basic cascade with an additional inhibitor binding reaction captured both features of this response (Figure 4F). While these results are similar to those observed under ERK phosphatase co-expression, the mechanisms behind enzymatic and binding-mediated regulation are different. CI-1040 effectively lowers the concentration of available MEK, thereby reducing the ultrasensitivity and increasing the threshold. The converse effect is seen in the variable cascade, in which increasing MEK concentration results in greater steepness and a lower response threshold.

Integrating Variable Expression Cascades with Negative Regulation

Our computational model captures all of the qualitative trends seen in the experimental data for individual perturbations to the basic synthetic cascade. We therefore used the model to probe the effects of combining different perturbations over a broader range of parameters. Initially, we explored the intrinsic perturbation of concentration variation within the basic cascade (Figure 5A) as MEK and ERK were varied from 10nM to 2μM and 10nM to 10μM, respectively, and the Hill coefficient, EC50 and signal strength were determined over the entire parameter space. Strikingly, the Hill coefficient is strongly biphasic, while the EC50 and signal strength are monotonic. This enables the decoupling of ultrasensitivity from other signal characteristics, simply by adjusting the relative concentrations of cascade members. For example, at high MEK concentrations, the EC50 is low and the signal strength is high, while the Hill coefficient can be independently tuned from approximately 2 to 4 by varying the ERK concentration. Conversely, at low MEK levels, the Hill coefficient is low for all ERK concentrations, while the EC50 and signal strength vary considerably as a function of ERK level. The decoupling of signal characteristics in the absence of extrinsic perturbation highlights the inherent flexibility in a three-tiered kinase cascade.

We then applied the extrinsic perturbation of MEK inhibition (Figure 5B) and found that the Hill coefficient is also biphasic with ERK, yet the transitions become steeper with respect to MEK concentration. The threshold is shifted so that, for low MEK, the EC50 is high for a larger range of ERK concentration than in the unregulated case. Not surprisingly, the region of maximal signal strength is smaller, showing a marked reduction in gain for low MEK and low ERK concentrations. We show in Figure 4 that two modes of inhibition were similar for given parameter values; however, modeling negative regulation with ERK phosphatase reveals very different behavior from binding inhibition of MEK when surveyed over a wider parameter space (Figure 5C). Though experimentally we see a decrease in ultrasensitivity upon phosphatase co-expression (Figure 4B,C), our model predicts that in a different region of parameter space the Hill coefficient will be greater than that of the basic cascade alone. Furthermore, in the presence of phosphatase, the EC50 becomes biphasic and the signal strength exhibits a broad range of intermediate values. These non-monotonic profiles increase the possible combinations of signal characteristics and further enable the decoupling of signal aspects.

Theoretical Analysis of Cascade-Generated Ultrasensitivity

Several mechanisms leading to MAPK ultrasensitivity have been posited including zeroth-order ultrasensitivity (Goldbeter and Koshland, 1981), dual-step phosphorylation, and competitive inhibition (Ferrell, 1996). Our synthetic cascade is not subject to either zeroth-order ultrasensitivity or competitive inhibition, but it is affected by dual-step phosphorylation of MEK and ERK. Interestingly, our experimental and computational results both indicate that kinase concentration itself, even in the absence of zeroth-order effects, contributes to MAPK ultrasensitivity (Figures 2 and 5). Therefore, we simulated dual-step and single-step mass-action kinetic models over a wide range of concentrations to dissect the contributions of multi-step processes and relative kinase concentration to the overall ultrasensitivity of ERK activation (Figure 6A). Additionally, we generated a Hill equation that matched the dose-response of active MEK from these explicit models and used this aggregate equation as the stimulus to a final, explicit ERK step. The relative kinase concentrations chosen correspond to distinct sets of behaviors identified in Figures S4 and S5.

We found that in all cases the ultrasensitivity arising from explicit cascading is greater than simple multiplicative accumulation (Figure 6B). Furthermore, when each level in the cascade is modeled as a single phosphorylation process (*i.e.*, when dual-step phosphorylation is eliminated) the supermultiplicative generation of ultrasensitivity by cascading is maintained and is strongly influenced by concentration, though the overall ultrasensitivity is considerably lower than that of dual-step cascades. To explore the mechanisms underlying this generation of ultrasensitivity by cascading, we analyzed the dose-response curves of each species accounted for by mass-action kinetics (Table S2). When the cascade is modeled explicitly, active MEK exists in either a free or complex-bound state and the behavior of these distinct species varies dramatically depending on the relative enzyme and substrate concentrations. For example, when the ultrasensitivity of ERK is high, this steepness arises specifically from the complex-bound MEK species, even though the total MEK ultrasensitivity is low (Figure 6C). In contrast, when the ERK ultrasensitivity is low there is a negligible difference between the dose responses of each MEK species as all have low ultrasensitivity. Notably, this phenomenon occurs for both dual-step and single-step kinase activation. Furthermore, when the Raf and MEK levels of the cascade are aggregated into a single Hill equation that accurately mimics the dose response of total active MEK in the explicit model, the complex-bound MEK species has a lower ultrasensitivity than in the explicit model alone (Figure 6D). Therefore, the multi-tiered structure of MAPK cascades does not simply serve to accumulate ultrasensitivity multiplicatively but it can actually generate ultrasensitivity *de novo* in a concentration-dependent manner through a distribution of intermediate species. An explicit model that accounts for all physiologically relevant species, without simplifying assumptions (*i.e.*, Hill equation and Michaelis-Menten approximations) or the inclusion of phosphatases, captures this previously unidentified mechanism of ultrasensitivity.

MEK Inhibition of the Variable Cascade

Based on our computational model we predicted that applying 50nM CI-1040 to the high-MEK variable cascade would decrease the ultrasensitivity, increase the threshold, and leave the signal strength unaffected. This is in contrast to the basic cascade in which the signal strength is predicted to be significantly lower upon MEK inhibition. As shown in Figure 5, both the basic and variable cascades are in the high signal strength region in the absence of MEK inhibition, yet with inhibition they are separated by a sharp transition from low to high signal strength. In this parameter regime, the Hill coefficient and EC50 become decoupled from the signal strength of the system. Therefore, we tested MEK inhibition in the variable cascade and observed a reduction in ultrasensitivity from $n_H = 2.8 \pm 0.19$ to 1.7 ± 0.17 and

an increase in EC50 from 6.6 ± 0.14 nM to 16 ± 1.1 nM (Figure 7A) as predicted by the model (Figure 7B). Strikingly, the basic cascade shows a significant reduction in signal strength, to ~25% uninhibited levels (Figure 7C,D) while the response of the variable cascade is unaffected by MEK1 inhibition (Figure 7E,F). These computational and experimental results demonstrate both the ability to decouple signal characteristics and the great degree of plasticity exhibited by the MAPK topology itself through the use of multiple, relatively simple, perturbations.

DISCUSSION

In this study, we used a synthetic biology approach to explore factors regulating the systems-level properties of a minimal MAPK module. Synthetic biology is a rapidly evolving discipline that has both engineered novel biological functions and contributed to the current understanding of natural processes (Grunberg et al., 2010; Hasty et al., 2002; Khalil and Collins, 2010; Kiel et al., 2010; Sprinzak and Elowitz, 2005). By reconstructing a biological system, applying perturbations and measuring the response, we can test and expand our understanding of how the system works and gain insight into how to modify it. Well-defined synthetic systems obviate some of the difficulties of natural systems that have an inherent degree of uncertainty with respect to molecules and topology. We used yeast as an *ex vivo* system to build a purely exogenous protein interaction network based on the mammalian ERK1/2 pathway. We also used mechanistic computational modeling to directly demonstrate conceptually new behaviors, such as cascade-based generation and concentration-based tuning of ultrasensitivity, independent of any experimental system.

Our simple synthetic cascade was used to investigate the role of scaffolding in shaping the activation profile of ERK. In contrast to the prozone effect, we see a monotonic dependence on scaffold concentration in which the signal strength is strong when the scaffold is either absent or expressed at optimal stoichiometric ratios, and greatly attenuated at high scaffold concentrations. Our data show that the synthetic cascade is catalytically efficient and therefore this monotonic response occurs because the cascade is not aided by the presence of scaffold. The disruption of signal strength seen at high scaffold concentrations can arise through multiple mechanisms, including combinatorial inhibition or dampened amplification. Combinatorial inhibition occurs when individual kinases become sequestered on separate scaffold molecules as has been posited experimentally for the KSR1 and JIP1/2 scaffolds (Burack and Shaw, 2000) and computationally for a generic two-member scaffold (Levchenko et al., 2000). More recent theoretical work on the MAPK cascade found that scaffolds lower the amplification and magnitude of a signal under conditions conducive to signal transduction in the absence of scaffold (Locasale et al., 2007). This effect was mediated entirely by dampening of amplification through the cascade and did not involve combinatorial inhibition.

We demonstrated that varying the relative concentrations of proteins intrinsic to the three-tiered MAPK module enables great flexibility of the system response and that key signal characteristics can be decoupled under certain parameter regimes (Figures 5 and 7). This suggests a potential cellular strategy for tuning the response of the MAPK cascade in distinct biological contexts without changing the module topology itself. Controlling protein expression levels through either gene expression or post-translational modification presents an effective and robust method for varying the activation profile of MAP kinases. Groundbreaking work on ultrasensitivity in the *Xenopus* oocyte Mos-MEK-p42 MAPK cascade revealed a sharply switch-like, irreversible response (Xiong and Ferrell, 2003). Interestingly, the relative concentrations of these proteins (Mos: 3nM, MEK: 1200nM, p42-MAPK: 330nM) (Ferrell, 1996) map the system to the high ultrasensitivity region of our theoretical heat map (Figure 5, marked X). In contrast, the Ste11-Ste7-Fus3 MAPK cascade

of the pheromone pathway in yeast has been shown to exhibit a less ultrasensitive activation profile (Hao et al., 2008; Poritz et al., 2001). Strikingly, the relative concentrations of these proteins (Ste11: 41nM, Ste7: 37nM, Fus3: 470nM) (Ghaemmaghami et al., 2003) place this cascade in the low ultrasensitivity region of our theoretical framework (Figure 5, marked Y). While it is clear that factors extrinsic to the module, such as positive feedback, scaffolding and subcellular compartmentalization, play important roles in determining the activation profile of these natural signaling cascades, these systems may be primed for their respective behaviors through the intrinsic parameter of kinase concentration.

We also identified kinase cascading as a novel mechanism for *de novo* generation of ultrasensitivity, and we showed that this effect is strongly concentration dependent, though it is not mediated by zeroth-order ultrasensitivity or solely by dual-step phosphorylation. We used a mass-action kinetic model, based largely on the seminal work of Huang and Ferrell (1996), to explore the role of cascading in generating ultrasensitivity. The model presented in their work specifically accounted for dual-step dephosphorylation at each level of the cascade and was therefore subject to heightened ultrasensitivity through an additional dual-step process and through zeroth-order ultrasensitivity by creation of an activation-deactivation cycle. We systematically deconstructed this model, first removing phosphatases and then simulating activation of each kinase as a single-step reaction; by eliminating these additional sources of ultrasensitivity, we were able to analyze the inherent contributions of the kinase-cascading architecture in generating MAPK ultrasensitivity. We found that over a broad range of relative kinase concentrations the steepness of each subsequent tier increases in a greater-than-multiplicative manner. This result was surprising as previous theoretical studies (Brown et al., 1997; Ferrell, 1997) suggest that the ultrasensitivity of sequential levels in a cascade accumulates in a multiplicative or submultiplicative manner. In contrast, our analysis shows that instead of simply passing steepness from one level to the next, cascading can lead to an output response whose Hill coefficient is greater than the product of the coefficients of the previous levels (Figure 6). The difference between our analysis and previous work arises because earlier models relied essentially on independent, though sequential, Hill equations in which there is one output species for a given input stimulus concentration. In our analysis, each level of the cascade contains a distribution of species (*i.e.*, different phosphorylation and complexation states) and the concentrations of these species depend on both the kinetic parameters of each reaction and the total concentrations of Raf, MEK and ERK. For a given input stimulus, this explicit apportioning of species results in a different output than the corresponding Hill equation approximation (Figure 6D), even at steady state, and the behaviors of these distinct species vary considerably as a function of concentration (Figure 6C).

Furthermore, a biphasic Hill coefficient is a prominent feature of concentration variation seen under all conditions (Figure 5). Ultrasensitivity is low when either MEK or ERK is limited and the extent of limitation for a given set of concentrations can be determined by the specific MEK species generated (Figures S4 and S5). The optimum Hill coefficient will depend not only on the molarity of the individual kinases but on parameters of activation as well. Previous work has shown that introducing compensatory alterations in the association and dissociation rate constants of Ras-Raf binding has a significant impact on the activation profile of ERK (Kiel and Serrano, 2009). Moreover, the influence of these different parameters is cell-type specific, indicating that the plasticity of MAPK signaling is multifaceted.

The steepness and magnitude of the biphasic Hill coefficient become enhanced through the addition of a phosphatase (Figure 5C) because of the introduction of an activation/deactivation cycle. The mechanism of dephosphorylation is also non-processive (Zhao and Zhang, 2001) and can contribute to the ultrasensitivity of the response. Additionally, the

generation of a cycle may further increase ultrasensitivity through zeroth-order effects in this region of parameter space. Interestingly, the addition of a cycle also results in a biphasic profile for the EC50 that is in contrast to MEK inhibition, in which no enzymatic cycle is created. Under MEK inhibition, the response is similar to that of the unregulated system but the region boundaries become shifted creating further opportunities to independently tune certain signal characteristics. We demonstrated experimentally that the signal strength of the system can be decoupled from the EC50 and Hill coefficient (Figure 7) and identify additional opportunities for isolating distinct signal features through this theoretical analysis.

Looking across each signal characteristic for different modes of regulation (Figure 5), it becomes apparent that some combinations of features are possible while others do not arise (Table S1). We find that for a low Hill coefficient, any combination of other signal aspects is attainable. However, to achieve a steep ultrasensitivity, the cascade must signal efficiently which requires that the EC50 be low and the signal strength be high. To build a MAPK cascade with a sharply switch-like response and a high threshold, additional modes of regulation must be employed. From a synthetic biology perspective, this type of analysis is useful in designing novel signaling cascades. For example, several research groups have successfully engineered endogenous receptors with altered specificity (Dwyer et al., 2003;Looger et al., 2003) or expressed exogenous receptors (Chen and Weiss, 2005) that recognize novel ligands and relay the signal through endogenous pathways. We have identified mechanisms for tuning the threshold and ultrasensitivity of a ubiquitous relay module and therefore these principles may be useful in altering biosensor sensitivity, building kinase-based logic gates, or tuning native signaling responses (such as differentiation, survival, or apoptosis) in engineering cells and tissues. Synthetic biology at the level of post-translational modification is currently at the cusp of rapid discovery and growth (Grunberg et al., 2010;Kiel et al., 2010). In this study, we have shown how the key signal characteristics of strength, threshold and ultrasensitivity in a ubiquitous and essential signaling module can be controlled through simple and accessible perturbations.

EXPERIMENTAL PROCEDURES

Plasmid and Strain Construction

Complete tables of plasmids and strains used in this study can be found in the Tables S3 and S4, respectively. All plasmid construction was done using standard cloning methods for PCR amplification, restriction digest, ligation and bacterial transformation. Integration vectors were derived from pRS403-6, and episomal vectors were derived from pESC-leu and pESC-ura (all from Stratagene). The anhydrotetracycline-regulated $tetO_7$ promoter and reverse tTA cDNA were cloned from pCM252 (EuroScarf). MKP-$1^{L16A/L17A}$ cDNA was obtained from Anton Bennett through Addgene plasmid 13478. Additional cDNAs were kindly provided by the following: His_6-ERK and c-myc-MEK from Natalie Ahn, eGFP:ΔRaf-1:ER-DD from Steen Hansen, c-myc-paxillin from Lloyd Cantley, the pTy1 promoter from Gerald Fink, and the YIL117c promoter from David Levin. $Paxillin^{Y118D}$ was generated by site-directed mutagenesis with standard PCR techniques and sequence verified. Yeast transformation was done with the LiAc method in selective synthetic complete dropout media. Single integration was confirmed by PCR screening of genomic DNA.

Growth and Induction

All strains were grown from a fresh colony in synthetic complete (SC) dropout media (0.67% yeast nitrogen base without amino acids, 2% glucose, 0.14% His-Leu-Trp-Ura dropout mix supplemented with appropriate amino acids) for 24 hours. Cells were grown with shaking at 30°C. Liquid culture was diluted into SC media with 2% galactose (no

glucose) and 0.5μg/ml aTC (Sigma Aldrich), and grown for 16 hours. One sample per estradiol titration was grown without aTC to determine the background. Cells were stimulated with β-estradiol (Sigma Aldrich) for 45 min for basic cascades and 120 min for variable cascades. For inhibitor experiments, cells were pre-treated for 30 min with CI-1040 (Axon Medchem) prior to estradiol stimulation. One ml cultures (OD_{660} = 0.7–0.8) were lysed for analysis by incubating them in 1ml fresh 0.1M NaOH at room temperature for 5 min. They were then resuspended in 50μl lysis buffer (120 mM Tris-HCl (pH 6.8), 10% glycerol, 4% SDS, 5% β-mercaptoethanol, 0.004% bromophenol blue) and incubated at 95°C for 3 min and frozen at −20°C. Estradiol titration was done in triplicate for each strain.

Quantitative Western Blotting and Analysis

Standard SDS-PAGE electrophoresis and transfer procedures were used. Primary antibodies used include anti-phospho-p44/42 MAP kinase (Cell Signaling Technology), anti-ERK (BD Biosciences), anti-α-tubulin (AbD Serotech), and anti-MEK (BD Biosciences). Secondary antibodies used with the Odyssey Infrared Imaging System (Li-Cor Biosystems) include goat-α-mouse-IRDye700DX (Rockland), goat-α-rabbit-IRDye800CW (Rockland), and donkey-α-rat-IRDye800CW (Rockland). Standard western blotting procedures were used with Odyssey blocking buffer (Li-Cor). Phospho-ERK intensity was normalized by total ERK signal or α-tubulin as loading controls.

Each individual experiment was log transformed and fit to a modified Hill equation (1) with a nonlinear least-squares method using Prism 4 software (GraphPad Software), and then normalized to the fitted baselines (R_o and R_{max}):

$$R=R_o+\frac{(R_{\max}-R_o)*L^{n_H}}{L^{n_H}+EC50^{n_H}}=R_o+\frac{(R_{\max}-R_o)}{1+\left(10^{(\log EC50-\log L)*n_H}\right)} \quad (1)$$

The left-hand equality is the standard Hill equation with lower and upper baselines R_o and R_{max}, respectively, R is the system response (signal strength), L is the ligand concentration, n_H is the Hill coefficient and $EC50$ is the half-maximal concentration of activation (threshold). The right-hand equality in Equation 1 is a rearrangement of the Hill equation that was used to fit log-transformed data. The normalized data for each strain were pooled, and the mean and standard error of the mean were calculated with Prism 4.

Transcriptional Activation of Endogenous Pathways

The minimal promoter of Fus1 (−266 to +1) fused to tdTomato was custom synthesized by Geneart with NotI and BamHI sites flanking the promoter region. Additional promoters, a modified pTy1 promoter amplified from BMH261 (Madhani and Fink, 1997) and the YIL117c promoter excised directly from p1366 (Jung et al., 2002), were subcloned into NotI and BamHI. Transformed strains were grown as above and stimulated with either β-estradiol for 2 hours or positive controls: 2.5μM α-factor for 2 hours (pheromone and cell wall integrity), glucose starvation for 4 hours (invasive growth), and 40mM caffeine for 6 hours (cell wall integrity). tdTomato expression was quantified by flow cytometry using a Guava flow cytometer (Millipore, Billerica, MA).

Model Formulation

We used an ordinary differential equation (ODE)-based, deterministic approach to model the basic cascade and its variations. In the basic cascade, protein synthesis, binding reactions, dual-step phosphorylation and protein degradation reactions were explicitly included. All binding and activation reactions were modeled with mass-action kinetics and did not rely on approximations of rapid equilibrium or pseudo-steady state (Michaelis-Menten). The series

of ODEs for each model was solved using the numerical stiff solver ode23s in MATLAB (The Mathworks). Steady-state response plots, as well as 3D surface and 2D phase plots, were generated in MATLAB. Further descriptions of the various model formulations are given in the Supplemental Text and model definitions, reactions, equations, parameters and initial conditions, are given in Tables S5–S9, respectively.

Supplementary Material

Refer to Web version on PubMed Central for supplementary material.

Acknowledgments

This work was supported by the National Institutes of Health (NIH) through the NIH Director's Pioneer Award Program, grant number DP1 OD00364, the Ellison Medical Foundation and the Howard Hughes Medical Institute (J.J.C), and by the American Heart Association, grant number 0835132N, and startup funds from the University of Pennsylvania (C.A.S). We also thank Natalie Ahn, Lloyd Cantley, Gerald Fink, Steen Hansen and David Levin for kindly providing cDNA.

REFERENCES

Atienza J. Human ERK1 Induces Filamentous Growth and Cell Wall Remodeling Pathways in Saccharomyces cerevisiae. J Biol Chem. 2000; 275:20638–20646. [PubMed: 10787425]

Avruch J. MAP kinase pathways: the first twenty years. Biochim Biophys Acta. 2007; 1773:1150–1160. [PubMed: 17229475]

Bagowski CP, Besser J, Frey CR, Ferrell JE Jr. The JNK cascade as a biochemical switch in mammalian cells: ultrasensitive and all-or-none responses. Curr Biol. 2003; 13:315–320. [PubMed: 12593797]

Bashor C, Helman N, Yan S, Lim W. Using Engineered Scaffold Interactions to Reshape MAP Kinase Pathway Signaling Dynamics. Science. 2008; 319:1539–1543. [PubMed: 18339942]

Bellí G, Garí E, Piedrafita L, Aldea M, Herrero E. An activator/repressor dual system allows tight tetracycline-regulated gene expression in budding yeast. Nucleic Acids Res. 1998; 26:942–947. [PubMed: 9461451]

Bhalla US, Ram PT, Iyengar R. MAP kinase phosphatase as a locus of flexibility in a mitogen-activated protein kinase signaling network. Science. 2002; 297:1018–1023. [PubMed: 12169734]

Brown GC, Hoek JB, Kholodenko BN. Why do protein kinase cascades have more than one level? Trends Biochem Sci. 1997; 22:288. [PubMed: 9270298]

Burack WR, Shaw AS. Signal transduction: hanging on a scaffold. Curr Opin Cell Biol. 2000; 12:211–216. [PubMed: 10712921]

Burack WR, Sturgill TW. The activating dual phosphorylation of MAPK by MEK is nonprocessive. Biochemistry. 1997; 36:5929–5933. [PubMed: 9166761]

Chen M, Weiss R. Artificial cell-cell communication in yeast Saccharomyces cerevisiae using signaling elements from Arabidopsis thaliana. Nat Biotechnol. 2005; 23:1551–1555. [PubMed: 16299520]

Chen R, Thorner J. System biology approaches in cell signaling research. Genome Biol. 2005; 6:235. [PubMed: 16207364]

Cullen PJ, Sprague GF Jr. Glucose depletion causes haploid invasive growth in yeast. Proc Nat Acad Sci USA. 2000; 97:13619–13624. [PubMed: 11095711]

Dwyer MA, Looger LL, Hellinga HW. Computational design of a Zn2+ receptor that controls bacterial gene expression. Proc Nat Acad Sci USA. 2003; 100:11255–11260. [PubMed: 14500902]

Elion EA. The Ste5p scaffold. J Cell Sci. 2001; 114:3967–3978. [PubMed: 11739629]

Ferrell J, Xiong W. Bistability in cell signaling: How to make continuous processes discontinuous, and reversible processes irreversible. Chaos. 2001; 11:227–236. [PubMed: 12779456]

Ferrell JE. Tripping the switch fantastic: how a protein kinase cascade can convert graded inputs into switch-like outputs. Trends Biochem Sci. 1996; 21:460–466. [PubMed: 9009826]

Ferrell JE. How responses get more switch-like as you move down a protein kinase cascade. Trends Biochem Sci. 1997; 22:288–289. [PubMed: 9270299]

Ferrell JE, Machleder EM. The biochemical basis of an all-or-none cell fate switch in Xenopus oocytes. Science. 1998; 280:895–898. [PubMed: 9572732]

Gao XD, Caviston JP, Tcheperegine SE, Bi E. Pxl1p, a paxillin-like protein in Saccharomyces cerevisiae, may coordinate Cdc42p and Rho1p functions during polarized growth. Mol Biol Cell. 2004; 15:3977–3985. [PubMed: 15215315]

Ghaemmaghami S, Huh WK, Bower K, Howson RW, Belle A, Dephoure N, O'Shea EK, Weissman JS. Global analysis of protein expression in yeast. Nature. 2003; 425:737–741. [PubMed: 14562106]

Goldbeter A, Koshland DE. An amplified sensitivity arising from covalent modification in biological systems. Proc Natl Acad Sci USA. 1981; 78:6840–6844. [PubMed: 6947258]

Grunberg R, Ferrar TS, van der Sloot AM, Constante M, Serrano L. Building blocks for protein interaction devices. Nucleic Acids Res. 2010; 38:2645–2662. [PubMed: 20215443]

Hao N, Nayak S, Behar M, Shanks R, Nagiec M, Errede B, Hasty J, Elston T, Dohlman H. Regulation of Cell Signaling Dynamics by the Protein Kinase-Scaffold Ste5. Mole Cell. 2008; 30:649–656.

Harding A, Tian T, Westbury E, Frische E, Hancock JF. Subcellular localization determines MAP kinase signal output. Curr Biol. 2005; 15:869–873. [PubMed: 15886107]

Hartwell LH, Hopfield JJ, Leibler S, Murray AW. From molecular to modular cell biology. Nature. 1999; 402:C47–52. [PubMed: 10591225]

Hasty J, Mcmillen D, Collins J. Engineered gene circuits. Nature. 2002; 420:224–230. [PubMed: 12432407]

Heinrich R, Neel BG, Rapoport TA. Mathematical models of protein kinase signal transduction. Mole Cell. 2002; 9:957–970.

Hornberg J, Bruggeman F, Binder B, Geest C, De Vaate A, Lankelma J, Heinrich R, Westerhoff H. Principles behind the multifarious control of signal transduction. ERK phosphorylation and kinase/phosphatase control. FEBS J. 2005; 272:244–258. [PubMed: 15634347]

Huang CY, Ferrell JE. Ultrasensitivity in the mitogen-activated protein kinase cascade. Proc Natl Acad Sci USA. 1996; 93:10078–10083. [PubMed: 8816754]

Ishibe S, Joly D, Zhu X, Cantley LG. Phosphorylation-dependent paxillin-ERK association mediates hepatocyte growth factor-stimulated epithelial morphogenesis. Mole Cell. 2003; 12:1275–1285.

Jung US, Sobering AK, Romeo MJ, Levin DE. Regulation of the yeast Rlm1 transcription factor by the Mpk1 cell wall integrity MAP kinase. Mol Microbiol. 2002; 46:781–789. [PubMed: 12410835]

Khalil AS, Collins JJ. Synthetic biology: applications come of age. Nat Rev Genet. 2010; 11:367–379. [PubMed: 20395970]

Kiel C, Serrano L. Cell type-specific importance of ras-c-raf complex association rate constants for MAPK signaling. Sci Signal. 2009:ra38. [PubMed: 19638615]

Kiel C, Yus E, Serrano L. Engineering signal transduction pathways. Cell. 2010; 140:33–47. [PubMed: 20085704]

Kolch W. Coordinating ERK/MAPK signalling through scaffolds and inhibitors. Nat Rev Mol Cell Biol. 2005; 6:827–837. [PubMed: 16227978]

Levchenko A, Bruck J, Sternberg PW. Scaffold proteins may biphasically affect the levels of mitogen-activated protein kinase signaling and reduce its threshold properties. Proc Natl Acad Sci USA. 2000; 97:5818–5823. [PubMed: 10823939]

Locasale J, Shaw A, Chakraborty A. Scaffold proteins confer diverse regulatory properties to protein kinase cascades. Proc Natl Acad Sci USA. 2007; 104:13307–13312. [PubMed: 17686969]

Looger LL, Dwyer MA, Smith JJ, Hellinga HW. Computational design of receptor and sensor proteins with novel functions. Nature. 2003; 423:185–190. [PubMed: 12736688]

Mackeigan JP, Murphy LO, Dimitri CA, Blenis J. Graded mitogen-activated protein kinase activity precedes switch-like c-Fos induction in mammalian cells. Mol Cell Biol. 2005; 25:4676–4682. [PubMed: 15899869]

Madhani HD, Fink GR. Combinatorial control required for the specificity of yeast MAPK signaling. Science. 1997; 275:1314–1317. [PubMed: 9036858]

Marshall CJ. Specificity of receptor tyrosine kinase signaling: transient versus sustained extracellular signal-regulated kinase activation. Cell. 1995; 80:179–185. [PubMed: 7834738]

McMahon M. Steroid receptor fusion proteins for conditional activation of Raf-MEK-ERK signaling pathway. Methods Enzymol. 2001; 332:401–417. [PubMed: 11305114]

Natarajan M, Lin K, Hsueh R, Sternweis P, Ranganathan R. A global analysis of cross-talk in a mammalian cellular signalling network. Nat Cell Biol. 2006; 8:571–580. [PubMed: 16699502]

Ohren JF, Chen H, Pavlovsky A, Whitehead C, Zhang E, Kuffa P, Yan C, McConnell P, Spessard C, Banotai C, et al. Structures of human MAP kinase kinase 1 (MEK1) and MEK2 describe novel noncompetitive kinase inhibition. Nat Struct Mol Biol. 2004; 11:1192–1197. [PubMed: 15543157]

Poritz MA, Malmstrom S, Kim MK, Rossmeissl PJ, Kamb A. Graded mode of transcriptional induction in yeast pheromone signalling revealed by single-cell analysis. Yeast. 2001; 18:1331–1338. [PubMed: 11571757]

Qi M. MAP kinase pathways. J Cell Sci. 2005; 118:3569–3572. [PubMed: 16105880]

Santos S, Verveer P, Bastiaens P. Growth factor-induced MAPK network topology shapes Erk response determining PC-12 cell fate. Nat Cell Biol. 2007; 9:324–330. [PubMed: 17310240]

Sprinzak D, Elowitz M. Reconstruction of genetic circuits. Nature. 2005; 438:443–448. [PubMed: 16306982]

Whitehurst A, Cobb MH, White MA. Stimulus-coupled spatial restriction of extracellular signal-regulated kinase 1/2 activity contributes to the specificity of signal-response pathways. Mol Cell Biol. 2004; 24:10145–10150. [PubMed: 15542825]

Wu JJ, Zhang L, Bennett AM. The noncatalytic amino terminus of mitogen-activated protein kinase phosphatase 1 directs nuclear targeting and serum response element transcriptional regulation. Mol Cell Biol. 2005; 25:4792–4803. [PubMed: 15899879]

Xiong W, Ferrell J. A positive-feedback-based bistable `memory module' that governs a cell fate decision. Nature. 2003; 426:460–465. [PubMed: 14647386]

Zhao Y, Zhang ZY. The mechanism of dephosphorylation of extracellular signal-regulated kinase 2 by mitogen-activated protein kinase phosphatase 3. J Biol Chem. 2001; 276:32382–32391. [PubMed: 11432864]

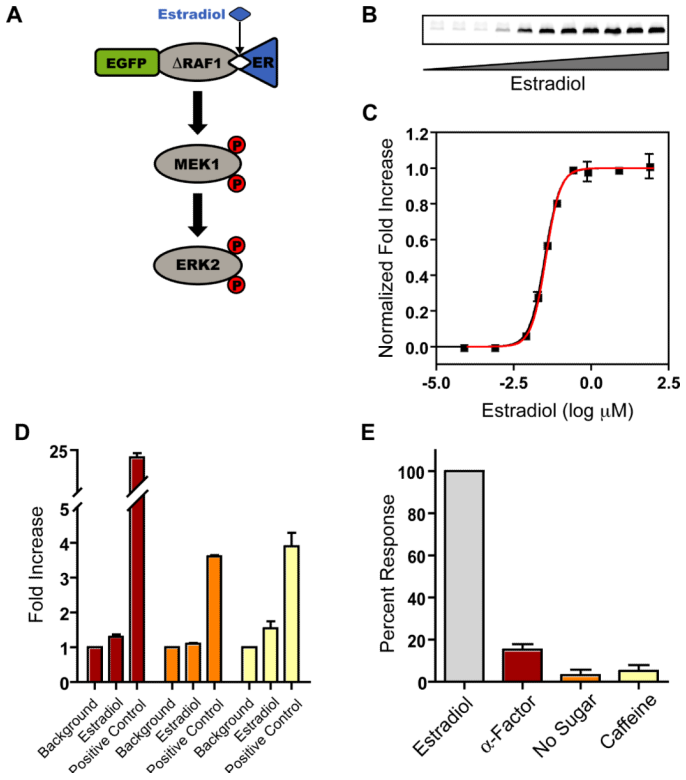

Figure 1. The Basic Synthetic Cascade

A. Schematic of the basic synthetic cascade. Raf:ER, MEK, and ERK were co-expressed by P_{tetO7}. The kinase activity of Raf:ER is modulated by estradiol. See also Figure S1A.

B. Representative western blot of steady-state ERK activation with increasing estradiol concentration.

C. ERK activation in response to estradiol titration (black squares). The experimental data are the mean ± SEM normalized to the fitted baselines. Data were fit with a modified Hill equation (black line). The model simulation results of the steady-state response profile for the basic cascade are shown as a red line. The system response is moderately ultrasensitive with a Hill coefficient of 1.8 ± 0.13 and an EC50 of 32 ± 1.4nM.

D. Transcriptional activation of endogenous promoters by the basic synthetic cascade. The data are the mean ± SEM tdTomato expression for the mating (red), invasive growth (orange) and cell wall integrity (yellow) pathways normalized to background.

E. Activation of ERK by endogenous stimuli. Data are the mean ± SEM phosphorylation level normalized to the estradiol stimulated cascade. See also Figure S1B.

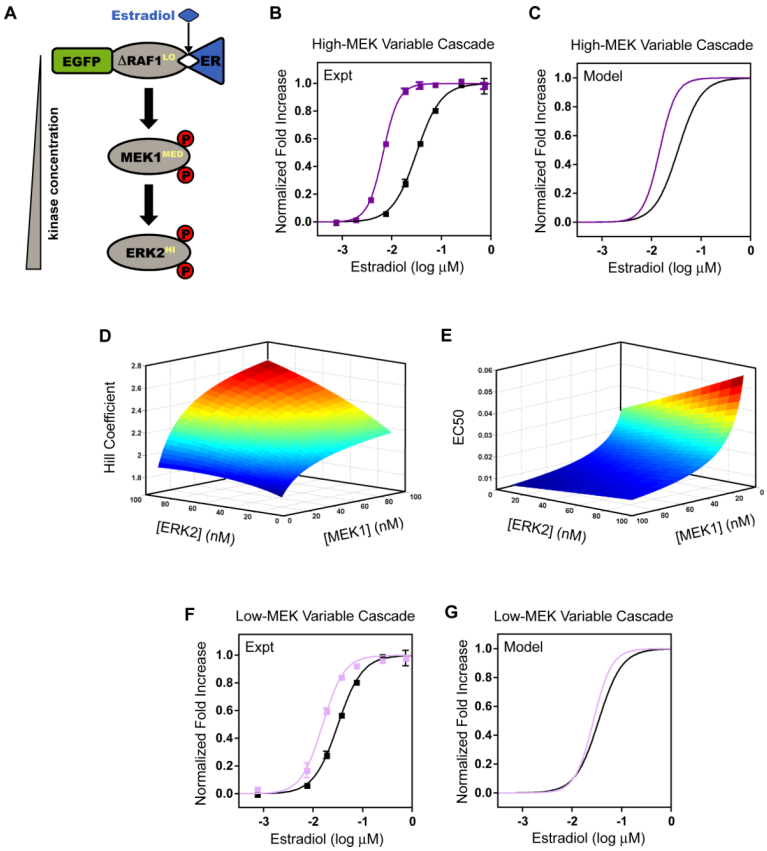

Figure 2. The Variable Expression Cascades

A. Schematic of variable expression cascades. The kinase concentration increases at each tier in the cascade.

B. Normalized fold increase of the high-MEK variable cascade (dark purple squares) and the basic cascade (black squares). The high-MEK variable cascade: single-copy Raf:ER expressed by P_{tetO7}, high-copy MEK expressed by P_{tetO7}, and high-copy ERK expressed by P_{Gal} (see also Figure S2). The data are the mean ± SEM, normalized to the fitted baselines. Data were fit with a modified Hill equation (solid lines).

C. Model simulations of the high-MEK variable cascade (dark purple) and the basic cascade (black). The fitted concentrations were Raf:ER = 10nM, MEK = 80nM, and ERK = 100nM.

D. Simulated Hill coefficient for the variable cascade in which both MEK and ERK were varied from 10nM to 100nM.

E. Simulated EC50 for the variable cascade for the same parameters as in D.

F. Normalized fold increase of the low-MEK variable cascade (light purple squares) and the basic cascade (black squares). The low-MEK variable cascade: single-copy Raf:ER expressed by P_{tetO7}, single-copy MEK expressed by P_{Gal}, and high-copy ERK expressed by P_{Gal}. The data are the mean ± SEM, normalized to the fitted saturation line. Data were fit with a modified Hill equation (solid lines).

G. Model simulations of the low-MEK variable cascade (light purple) and the basic cascade (black). The fitted concentrations were Raf:ER = 10nM, MEK = 30nM, and ERK = 100nM.

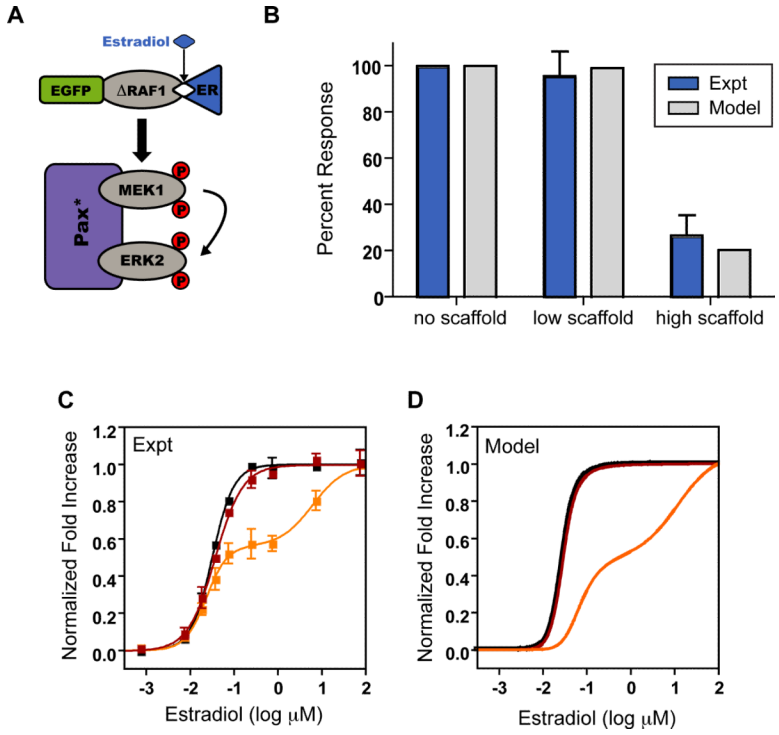

Figure 3. The Basic Cascade with Scaffolding

A. Schematic of the basic cascade co-expressed with a two-member scaffold pax*. See also Figure S3A.

B. Percent response of the basic cascade alone and co-expressed with single-copy or high-copy pax*. The experimental data (red) are the mean ± SEM and the computational data (grey) are single values. Both are normalized to the maximum activation of the basic cascade in the absence of scaffold.

C. Normalized fold increase of the basic cascade (black squares) co-expressed with single-copy (red squares) or high-copy (orange squares) pax*. The data are the mean ± SEM, normalized to the fitted baselines (basic and single-copy pax*) or the minimum and maximum values (high-copy pax*) for each condition. The data were fit with a modified Hill equation (black and red lines) or biphasic dose-response equation (orange line).

D. A compartmental model of no (black), low (red) or high (orange) scaffold expression. Simulations are normalized to the maximum value of each condition. See also Figure S3B.

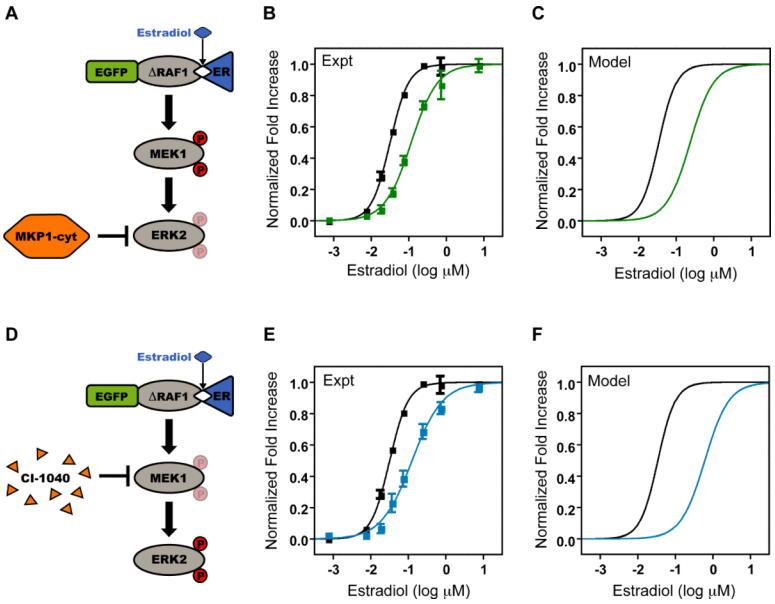

Figure 4. Negative Regulation of the Basic Cascade

A. Schematic of the basic cascade co-expressed with the ERK phosphatase MKP1-cyt.

B. Normalized fold increase of the basic cascade (black squares) co-expressed with high-copy MKP1-cyt (green squares) expressed by P_{Gal}. The data are the mean ± SEM, normalized to the fitted baselines. The data were fit with a modified Hill equation (solid lines).

C. Model simulations with (green) and without (black) MKP1-cyt co-expression. Data are normalized to the maximum value of each condition.

D. Schematic of the basic cascade with the MEK inhibitor CI-1040.

E. Normalized fold increase of the basic cascade (black squares) pre-treated with 50nM CI-1040 for 30 minutes prior to estradiol stimulation (blue squares). The data are the mean ± SEM, normalized to the fitted baselines. The data were fit with a modified Hill equation (solid lines).

F. Model simulations with (blue) and without (black) inhibitor pre-treatment. Data are normalized to the maximum value of each condition.

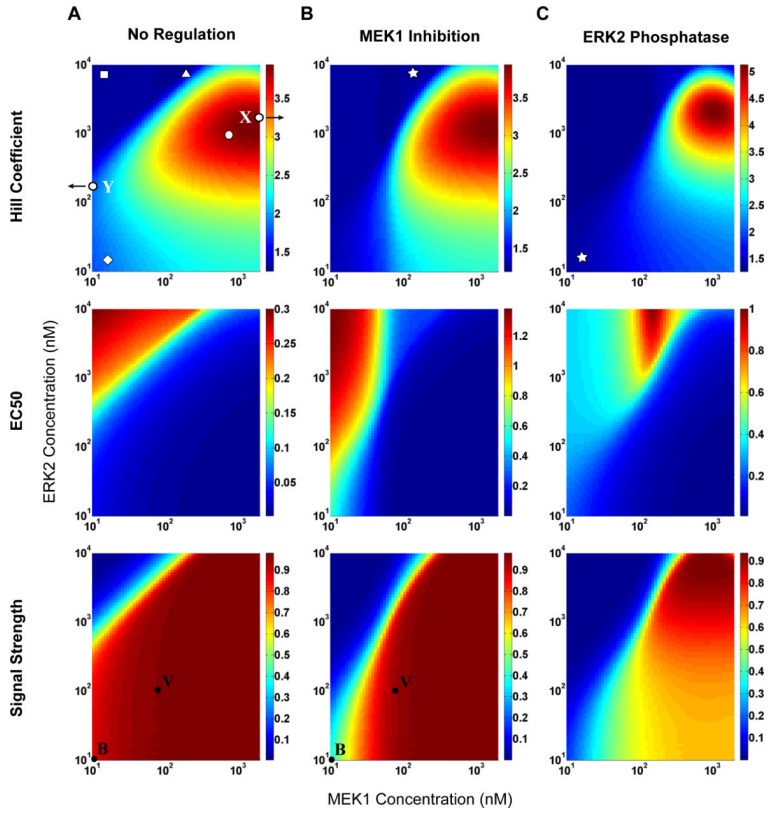

Figure 5. Computational Analysis of Concentration Variation and Negative Regulation

A. No regulation: Raf:ER was held constant at 10nM, and MEK and ERK were varied from 10nM to 2μM and 10nM to 10μM, respectively. The top panel shows the Hill coefficient, the middle panel shows the EC50, and the bottom panel shows the normalized signal strength. On the top panel, the point marked "X" indicates the *Xenopus* cascade and the point marked "Y" indicates the yeast pheromone cascade. Each symbol represents a distinct class of system response (Table S1). For example, the square identifies systems for which the Hill coefficient is low, the EC50 is high and the normalized signal strength is low. On the bottom panel, the point marked "B" denotes the basic cascade and the point marked "V" denotes the high MEK variable cascade. See also Figures S4 and S5.

B. MEK inhibition: The same parameter space as in A modeled with 50nM CI-1040. On the top panel, the star represents a distinct system response not seen in the absence of regulation. In the bottom panel, "B" indicates the basic cascade and "V" indicates the high-MEK variable cascade.

C. ERK phosphatase: The same parameter space as in A modeled with 100nM MKP1-cyt co-expression. The star represents the system response in B achieved in a different region of parameter space.

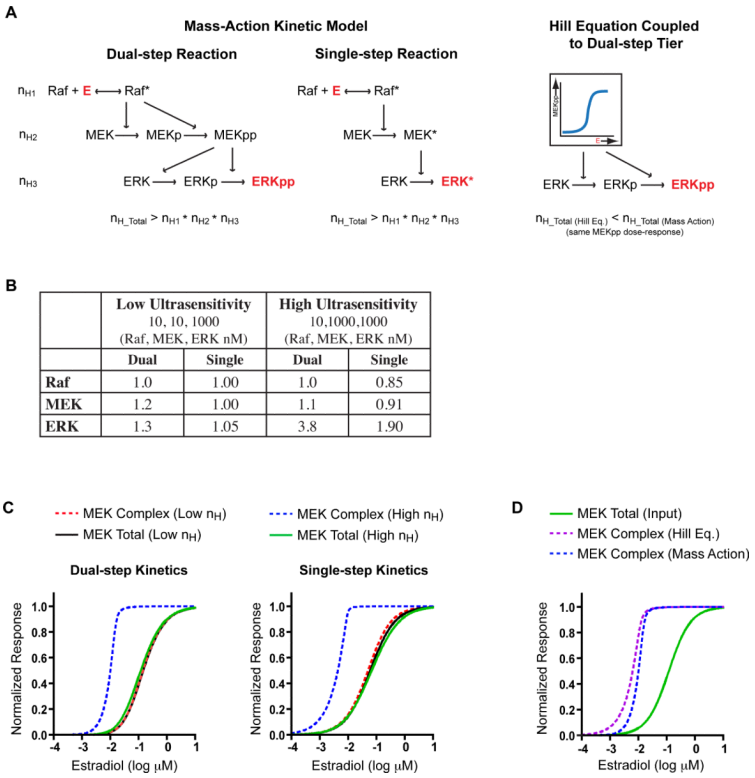

	Low Ultrasensitivity 10, 10, 1000 (Raf, MEK, ERK nM)		High Ultrasensitivity 10,1000,1000 (Raf, MEK, ERK nM)	
	Dual	**Single**	**Dual**	**Single**
Raf	1.0	1.00	1.0	0.85
MEK	1.2	1.00	1.1	0.91
ERK	1.3	1.05	3.8	1.90

Figure 6. Theoretical Analysis of Cascade-Generated Ultrasensitivity

A. Schematic of dual-step and single-step mass-action kinetic models and a lumped Hill equation model coupled to a dual-step tier.

B. The Hill coefficients of each level of the cascade for both dual- and single-step mass-action kinetic models for representative low and high ultrasensitivity systems. See also Table S2.

C. Simulations of distinct active MEK species for dual- and single-step cascades at the relative concentrations indicated in B.

D. Comparison of simulated active MEK complex species with the Hill equation and mass-action kinetic models for the same input function (total active MEK) in the high ultrasensitivity system.

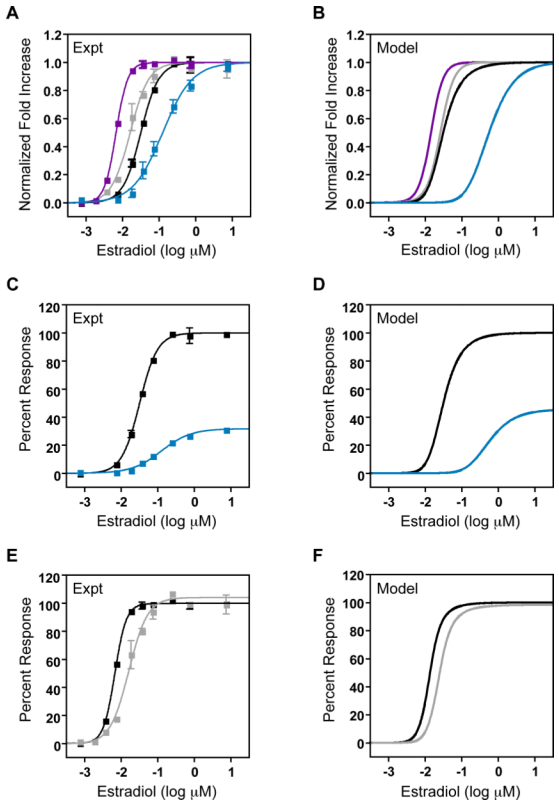

Figure 7. MEK Inhibition of the Variable Cascade

A. Normalized fold increase for the high-MEK variable cascade with (pink squares) and without (dark purple squares) pre-treatment with 50nM CI-1040 and for the basic cascade with (blue squares) and without (black squares) this inhibitor. The data are the mean ± SEM normalized to the fitted baselines for each condition. The data were fit with a modified Hill equation (solid lines).

B. Model simulations of the experimental conditions described in A.

C. Percent response of the basic cascade with (blue squares) and without (black squares) 50nM CI-1040 pre-treatment. The data are the mean ± SEM normalized to the maximum activation of the basic cascade in the absence of inhibitor.

D. Model simulations of the experimental conditions described in C.

E. Percent response of the high-MEK variable cascade with (pink squares) and without (black squares) 50nM CI-1040 pre-treatment. The data are the mean ± SEM normalized to the maximum activation of the high-MEK variable cascade in the absence of inhibitor.

F. Model simulations of the experimental conditions described in E.